

# Open-loop multi-channel inversion of room impulse response

*Bowon Lee, Camille Goudeseune, Mark A. Hasegawa-Johnson*

University of Illinois at Urbana-Champaign  
 {bowonlee,cog,jhasegaw}@illinois.edu

## Abstract

This paper considers methods for audio display in a CAVE-type virtual reality theater, a 3 m cube with displays covering all six rigid faces. Headphones are possible since the user’s headgear continuously measures ear positions, but loudspeakers are preferable since they enhance the sense of total immersion. The proposed solution consists of open-loop acoustic point control. The transfer function, a matrix of room frequency responses from the loudspeakers to the ears of the user, is inverted using multi-channel inversion methods, to create exactly the desired sound field at the user’s ears. The inverse transfer function is constructed from impulse responses simulated by the image source method. This technique is validated by measuring a  $2 \times 2$  matrix transfer function, simulating a transfer function with the same geometry, and filtering the measured transfer function through the inverse of the simulation. Since accuracy of the image source method decreases with time, inversion performance is improved by windowing the simulated response prior to inversion. Parameters of the simulation and inversion are adjusted to minimize residual reverberant energy; the best-case dereverberation ratio is 10 dB.

## 1. Introduction

The task of interest in this paper is free-field audio display for a virtual reality environment [1]. The virtual reality testbed for these experiments is a 3 m cube called ALICE (A Laboratory for Interactive Cognitive Experiments), located at the University of Illinois. Images are projected from outside onto all faces of the cube. Users are untethered: no wires connect equipment they wear to the outside world. In order to accurately convey images to the user, the positions of up to 20 user points (e.g., head, ears, hands, and feet) are precisely tracked using a magnetic tracking system (calibrated mean accuracy of 8 cm and 1 degree, 120 samples updated per second). The goal of virtual reality in ALICE is total immersion: users must be able to “suspend disbelief” and convince themselves that they are physically present in the virtual environment portrayed to them.

The goal of most previous virtual reality audio experiments is to correctly portray the position of a sound source. Position accuracy is usually achieved by filtering the audio signal through head-related

transfer functions and then playing it over headphones. The disadvantage of headphone audio is that it sounds like it is coming from the headphones. The impression of total immersion is lost if the audio display is part of the user's headgear rather than part of the environment.

A measure of headphone-free realism is possible by simply playing the desired audio from the most appropriate speaker in a large speaker array. For the ALICE environment, an array of eight transparent loudspeakers has been prototyped. These loudspeakers consist of millimeter-thick sheet glass suspended into the cube, connected to compression drivers located outside the walls of the cube. The transparent speakers provide reasonable audio display with good localization for distant objects (outside the cube wall), and most important, the transparent loudspeakers do not obstruct or distort the video display.

Moving the virtual audio source inside the room is much more difficult. The positions of the user's ears are known precisely. If the room impulse response were known, then the known room impulse response could be inverted using well-studied multi-channel inversion methods [2, 3], thus creating exactly the desired sound field at the two ears of the user. Unfortunately the room impulse response is not known. The user is free to put his or her head anywhere in the room; it is impossible to measure the room impulse response from every speaker location to every possible location of the user's ears.

Two solutions to this problem are possible. First, an estimate of the room impulse response can be adaptively updated using microphones placed on the user's headgear, by means of a number of adaptive signal processing methods. This paper analyzes a second solution to the problem of headphone-free virtual reality audio display. The proposed solution consists of open-loop acoustic point control, using a simulation of room impulse response based only on knowledge of the room geometry, architectural materials, and user location.

The image source method of room response simulation was originally proposed for open-loop dereverberation experiments similar to the one proposed here [4]. Its performance was never quantitatively reported in the literature, since multi-channel inversion methods for non-minimum phase impulse responses were not well understood at that time [5]. Other methods of simulating room impulse response are almost always evaluated by purely qualitative means like acoustic perceptual studies and visual comparisons of impulse responses [6].

This paper proposes instead to evaluate simulated room impulse responses based on their performance in a regularized dereverberation task. Dereverberation performance is measured in terms of the decibel ratio of the energy of the room impulse response to that of the dereverberated response. It is demonstrated that this method can be used to optimize parameters of the model including absorptivity and window taper.

This paper is organized as follows. Section 2 describes previous published research in the fields of room impulse response measurement, room impulse response simulation, and room impulse response inversion. Section 3 describes the methods of these tasks in a simulated virtual reality environment,

a 2 m plywood cube. Room impulse responses are measured with a starter pistol. An evaluation metric is proposed to quantitatively measure the dereverberation ratio. Section 4 discusses the results, demonstrating how the proposed evaluation metric optimizes methods for simulating and inverting the room impulse response. Section 5 reviews conclusions.

## 2. Background

### 2.1. Measurement of room impulse response

An excitation signal is required in order to measure a room impulse response. A perfect impulse (a Dirac delta function) simplifies the measurement task (measured response equals the impulse response), but it is not possible to physically generate a Dirac delta function. In practice, impulse-like signals or signals with characteristics similar to a perfect impulse such as flat frequency response are used.

ISO Standard 3382 specifies the following requirements for an excitation signal for measuring room impulse response [7]. First, it should be nearly omnidirectional. Second, its sound pressure level should provide sufficient dynamic range to avoid contamination by background noise. Third, the signal should be repeatable.

Impulse-like signals such as the starter pistol, balloon pop, and electric spark have been traditionally chosen as excitation signals [7, 8]. These impulses are easily generated and have been used to determine rough characteristics of a room, such as reverberation time. However, measurement by these impulse methods has not been widely discussed in the scientific literature for three reasons. First, the frequency response of these impulses is not flat (Fig. 1). Second, some authors report that it is difficult to get an adequate SNR because all the impulse's energy is packed into a very short duration [8]. Third, the signal is not precisely repeatable because it depends significantly on small variations in charge distribution, balloon shape, etc (Fig. 2).

In 1979 Schroeder suggested an alternative method to measure room impulse response using Maximum Length Sequences (MLS) [8]. The autocorrelation function of an MLS of order  $m$  with length  $N = 2^m - 1$  samples is two-valued, 1 at time zero and  $-1/N$  at times other than zero (modulo  $N$ ). If  $N$  is sufficiently large, then  $-1/N$  becomes negligible and we can assume that the resulting MLS has the same autocorrelation as pseudo-random noise. Because MLS signal energy grows with  $N$ , its SNR can be made arbitrarily high without needing high amplitude, which is not the case with impulses. Since the MLS is stored in a computer, it can be generated repeatedly. Therefore MLS meets the last two requirements of ISO 3382 better than impulse-like signals such as starter pistols and electric sparks.

Computer-generated pseudo-random sequences have discrete values such as  $+1$  and  $-1$ . Since it is impossible to make perfectly abrupt transitions between these two values, distortion occurs and the frequency response of the system must therefore be compensated to acquire accurate impulse responses.

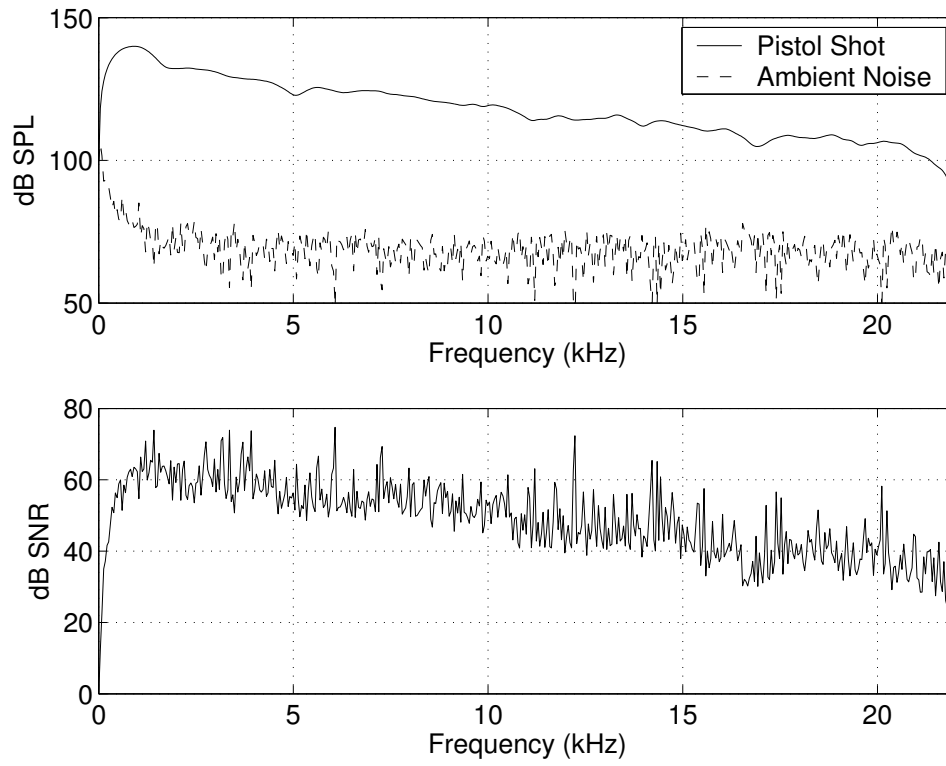


Fig. 1: Magnitude responses of starter pistol and ambient noise.

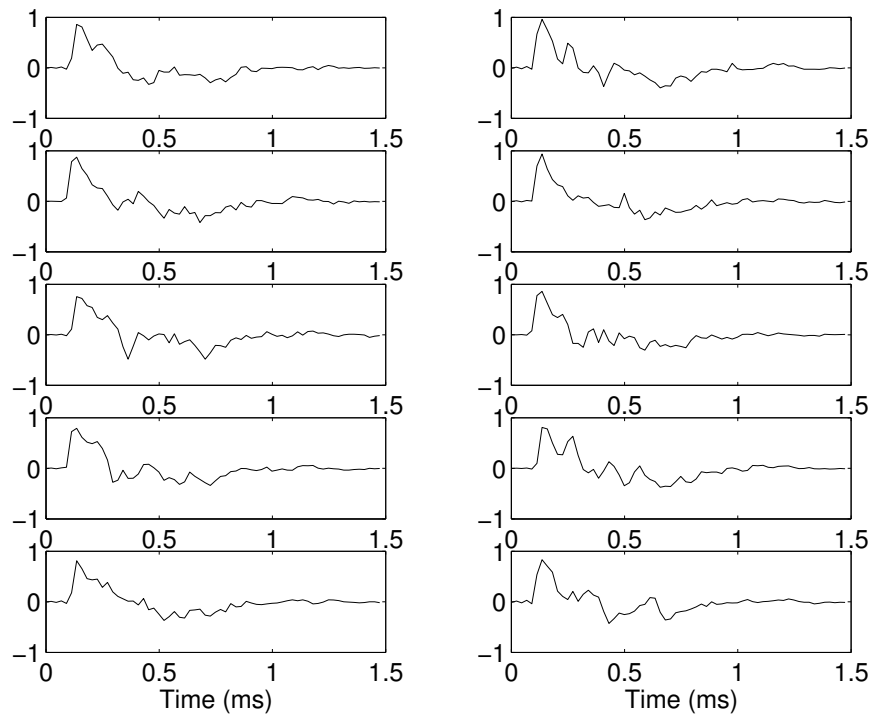


Fig. 2: Waveforms of individual pistol shots.

The technique of MLS measurement has also been proven to be vulnerable to the nonlinearity of measuring equipment, particularly loudspeakers [9]. Nonlinearities produce repeated distortion peaks in the time domain, which prevent the integrated energy of the impulse response from falling below  $-30$  dB [10, 11]. A modification of MLS, the inverse repeated sequence (IRS), reduces the distortion caused by nonlinearities [12, 13, 14]. Other papers discuss the accuracy of the MLS method [15, 16], its computational complexity [17, 18, 19, 20, 21], and its application to a variety of system response measurements [22, 23, 24].

Aoshima proposed the time-stretched pulses technique, based on the time expansion and compression of an impulsive signal [25]. The purpose of the time-stretched pulse signal is to increase the total energy of the excitation signal while keeping the frequency response flat.

Berkhous proposed a sine sweep as an excitation signal [26]. Farina and Ugolotti introduced a logarithmic sine sweep method using a different deconvolution method [27]. Farina's detailed method accurately derives an impulse response from the raw measurement by separating the linear and nonlinear components of the measured impulse response, where the strength of nonlinear distortion is measured by observing the harmonic distortion caused by nonlinearity of the system.

Stan *et al.* compare four different room impulse response measurement techniques: pseudo-random noise (MLS and IRS), time-stretched pulses, and logarithmic sine sweep [11]. Since the randomized phase of psuedo-random sequences makes them immune to background noise, MLS and IRS techniques are preferred in noisy environments. However, parameter optimization is required for high SNR because of nonlinear distortion. Nevertheless, the achieved SNR is only 60.5 dB with an MLS order of 16 and single measurement.

Time-stretched pulses and sine sweep methods produce a higher SNR than the pseudo-random noise techniques, but they require a quiet environment. The SNR of the time-stretched pulses technique is 77 dB after precise calibration. The logarithmic sine sweep method has 80.1 dB SNR. The benefit of the sine sweep is that unlike the previous methods, it produces a high SNR without any calibration [11].

## 2.2. Simulation of room impulse response

Simulations of room impulse responses fall into two categories: spatial mesh methods and ray acoustic methods.

Spatial mesh methods numerically solve the constituents of the acoustic wave equation, namely the equations of motion and continuity [28, 29]. In this method, sound pressure and velocity are computed at a finite number of points, usually mesh points in a cavity. The differential equations in the continuous domain are computed as difference equations in the discrete domain. This method can simulate diffraction effects, which ray acoustic methods cannot. Unfortunately, to compute an impulse

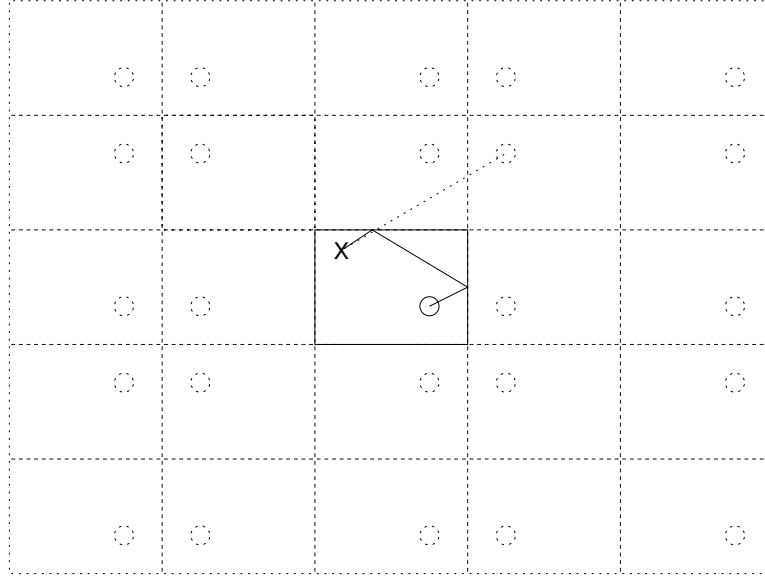


Fig. 3: Two-dimensional illustration of the image source method.; ‘x’=receiver, solid ‘o’=source, dashed ‘o’=image sources. Solid line=an echo path, dashed line=corresponding image source path.

response at a specific location of interest, the values of sound pressure and velocity must be computed over the entire mesh, because the solution at a specific point depends on those of the adjacent points. Spatial mesh methods are thus far more computationally expensive than ray acoustic methods.

Ray acoustic methods assume that sound rays are emitted from the sound source, usually as a spherical wave. Ray paths are then traced using either image source or ray-tracing methods [4, 30]. The ray-tracing method considers a finite number of rays to be emitted from the sound source. These ray paths are traced and their trajectories summed at points of interest. Although it requires little computation, ray tracing is appropriate only for a rough estimate, e.g., to compute the first few reflections of the room impulse response.

In 1979 Allen and Berkley showed that the impulse response of a small rectangular room can be computed using a geometric “image source” method [4]. Their model creates an “image space” without walls, in which each echo is modeled as the direct sound from an image source outside the actual walls of the room. The first six image sources are reflections of the original source in the six walls of the room. The next few image sources are created by reflecting the first six, and so on (Fig. 3). At each reflection, the amplitude of the source is scaled by the wall’s reflection coefficient.

The image source method requires more computation than ray tracing because it considers all possible reflected wavefronts. It can be extended from rectangular cavities to arbitrary polyhedra [31]. In this case, some image sources may not contribute to the total impulse response. Such image sources are called hidden images. An algorithm is therefore needed to decide whether a given image source is

hidden or not. Lee and Lee proposed a relatively efficient algorithm for the image source computation of impulse responses of arbitrarily shaped rooms [32], but this method is still computationally expensive relative to the image source method for rectangular rooms. The image source method is efficient for a rectangular room because every image source contributes to the total impulse response (unless there are obstacles in the room), and also, because the locations of all image sources are analytically pre-computed due to symmetry.

In a rectangular room, the image sources can be indexed by integer coordinates  $l$ ,  $m$ , and  $n$ , where  $(l, m, n) = (0, 0, 0)$  corresponds to the direct source,  $(1, 0, 0)$  corresponds to the first reflection in the positive  $x$  direction, and so on.

Given a room of size  $(L_x, L_y, L_z)$  with origin at the center and a source location  $(S_x, S_y, S_z)$ , the image source location with indices  $(l, m, n)$  is:

$$(I_x, I_y, I_z) = (lL_x + (-1)^l S_x, mL_y + (-1)^m S_y, nL_z + (-1)^n S_z)$$

Then the distance  $d_{lmn}$  from the image source to the receiver at  $(R_x, R_y, R_z)$  is:

$$d_{lmn} = \sqrt{(R_x - I_x)^2 + (R_y - I_y)^2 + (R_z - I_z)^2}$$

The impulse response predicted by the image source method is

$$g(t) = \sum_{l,m,n=-\infty}^{\infty} \frac{r^{|l|+|m|+|n|}}{d_{lmn}} \delta(t - \tau_{lmn}) \quad (1)$$

where  $\tau_{lmn} = d_{lmn}/c$  is the wave propagation time from the image source at  $(l, m, n)$  to the receiver,  $c$  is the speed of sound, and  $r$  is the reflection coefficient of the walls. Eq. (1) assumes that all surfaces have the same reflection coefficient, but relaxing this assumption is straightforward and computationally inexpensive.

Three-dimensional audio applications are usually considered in a rectangular cavity, a room; this paper considers only this special but common case, to justify use of the otherwise computationally expensive image source method for simulating the room impulse response.

### 2.3. Inversion of room impulse response

Given the room impulse response, a desired signal can be reproduced at points of interest if a valid inverse filter is first created from the impulse response. The dereverberation problem thus reduces to constructing such an inverse filter.

Since the purpose of inverting the room impulse response is to cancel reverberation at multiple points in a room, human ears for example, the frequency responses and inverse filters are formulated as a matrix of sequences. Let the term transfer function denote this matrix of frequency responses.

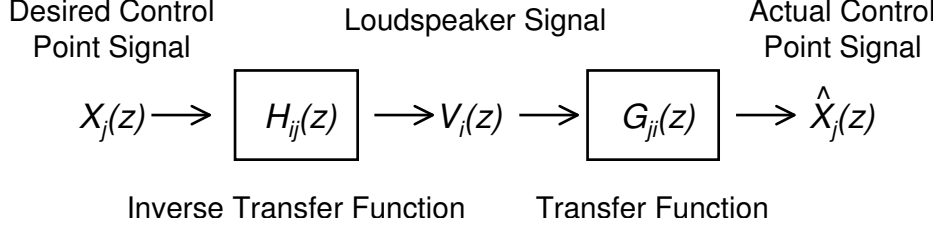


Fig. 4: System diagram.

Let  $G_{ji}(z)$  be the frequency response from the  $i^{th}$  loudspeaker to the  $j^{th}$  control point, for  $1 \leq i \leq L$  and  $1 \leq j \leq M$ : a total of  $M \times L$  individual room impulse responses. The inverse of this transfer function is therefore an  $L \times M$  matrix. The image source method computes the simulated frequency response  $\hat{G}_{ji}(z)$  which approximates  $G_{ji}(z)$ .

Let  $X_j(z)$  and  $\hat{X}_j(z)$  denote the Z-transforms of the desired and actual control point signals respectively. The inverse transfer function  $H(z)$  has as element  $H_{ij}(z)$ , the impulse response from the  $j^{th}$  desired control point signal  $X_j(z)$  to the  $i^{th}$  loudspeaker signal  $V_i(z)$ .  $\hat{X}_j(z)$  is therefore expressed as

$$\hat{X}_j(z) = \sum_i \hat{G}_{ji}(z) V_i(z) = \sum_{i,k} \hat{G}_{ji}(z) H_{ik}(z) X_k(z)$$

We want to find  $H_{ij}(z)$  so that  $\hat{X}_j(z)$  is as similar as possible to  $X_j(z)$ . Figure 4 shows the diagram of the room impulse response inversion process. If  $L = M$  and the matrix  $\hat{G}(z)$  is minimum phase, then an exact inverse transfer function is given by  $H(e^{j\omega}) = \hat{G}(e^{j\omega})^{-1}$ .

If the impulse responses are non-minimum phase, the inverse filter has poles outside the unit circle. In this case, we can make the inverse filter either stable but noncausal (the region of convergence includes the unit circle) or causal but unstable (the region of convergence does not include the unit circle), but not both stable and causal. Therefore, the exact inverse filter of a square transfer function matrix is only realizable for minimum phase transfer functions.

Neely and Allen found that the impulse response of a small room is minimum phase only for reflection coefficients below approximately 0.37 [5]. The impulse response of a small room is rarely minimum phase, and therefore the stable inverse filter  $\hat{G}(e^{j\omega})^{-1}$  of a square matrix  $\hat{G}(e^{j\omega})$  is usually noncausal in practice.

Miyoshi and Kaneda showed that the transfer function of a room can be exactly inverted for the case  $L = 2, M = 1$  [2]. Nelson *et al.* generalized their result by showing that, in most circumstances without any extreme symmetry, when  $L > M$ , the transfer function can be exactly inverted [33]. Thus a stable, causal inverse transfer function exists if  $G_{ji}(z)$  has more columns than rows. Unfortunately no tractable method for finding the causal, stable inverse of a non-square transfer function in the frequency domain has yet been proposed. An equivalent method can be computed in the time domain, but is



computationally expensive.

Recall that a non-minimum phase square transfer function has a stable but noncausal inverse  $H(e^{j\omega})$ . A causal, stable semi-inverse may be constructed by applying a time shift  $D$ :

$$\tilde{H}(e^{j\omega}) = e^{-j\omega D} H(e^{j\omega}) \quad (2)$$

and then truncating  $\tilde{h}[n]$  by zeroing the tail at  $n < 0$ :

$$\hat{h}[n] = \begin{cases} \tilde{h}[n], & n \geq 0 \\ 0, & n < 0 \end{cases} \quad (3)$$

This creates a stable and causal approximation  $\hat{h}[n]$  of the exact inverse filter. The time shift  $D$  is called modeling delay.

The inverse transfer function  $H$  can be computed by sampling the spectrum of  $\hat{G}$  using an FFT, and inverting the matrix at each frequency bin. Sampling the frequency-domain transfer function causes aliasing in the time domain. This “wrap-around effect” is eliminated by time-shifting  $h[n]$  by  $e^{-j\omega D}$ , which is the same as the modeling delay described previously.

Merely inverting the sampled FFT matrix  $\hat{G}$  yields a poor estimate of  $H$  because of singularities related to the non-minimum phase character of  $\hat{G}$  (zeros of  $\hat{G}$  tend to be very close to the unit circle). A better estimate can be computed by using a regularized inversion formula [3], in which a small constant  $\beta$  is added to each eigenvalue of  $G$  before inversion:

$$H = (\hat{G}^T \hat{G} + \beta I)^{-1} \hat{G}^T \quad (4)$$

where  $\hat{G}^T$  is the Hermitian transpose of  $\hat{G}$ .

After computing  $H(e^{j\omega})$  using Eq. (4), Eqs. (2) and (3) yield a stable and causal approximate inverse  $\hat{h}[n]$ . The resulting control point signal vector is

$$\hat{X} = G \hat{H} X$$

Signals produced during regularized inversion are depicted in Fig. 5. For illustration, a one-dimensional inverse transfer function is computed from the simulation  $\hat{G}$  and filtered through the simulated transfer function itself ( $\hat{X} = \hat{G} \hat{H} X$ ). Regularized inversion gives more than 50 dB of SNR with  $D = 750$  ms and  $\beta = 0.05$  (Fig. 5).

### 3. Methods

This section describes the design and validation of an open-loop room response inversion algorithm. Section 3.1 describes methods for acquiring validation data (measured room responses) using impulse-like excitation signals. Sections 3.2 and 3.3 describe methods for simulating and inverting the room response.

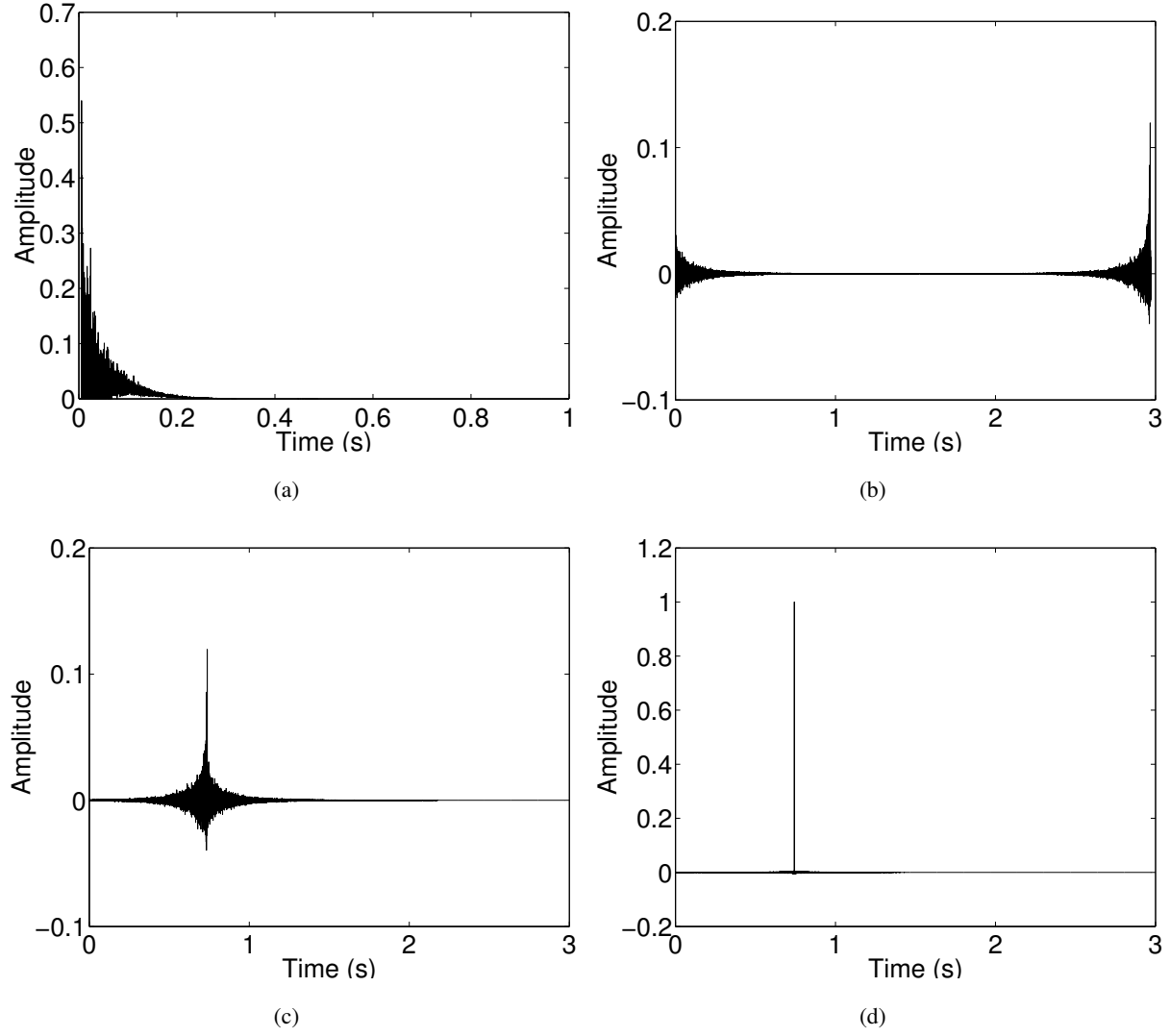


Fig. 5: Inversion process. (a), simulated impulse response  $\hat{g}(t)$ ; (b), noncausal inverse filter  $h(t)$  using regularized inversion; (c), shifted and truncated inverse filter  $\hat{h}(t)$ ; and (d), dereverberated output  $\hat{x}(t)$  ( $x(t) = \delta(t)$ ).

### 3.1. Room response measurement

Because of the deficiencies described in Section 2.1, few papers in recent decades describe impulse response measurement techniques using impulse-like excitation signals. For the application considered in this paper, impulse-like signals have important advantages. Measurement techniques were therefore developed to minimize their disadvantages.

#### 3.1.1. *Motivation for the use of starter pistol as an impulse*

Using a starter pistol for room response measurement has three advantages over non-impulse signals using loudspeakers. First, measured response need not be deconvolved into an impulse response because it is already qualitatively similar to the room impulse response. Second, the SNR is very high because the starter pistol exceeds 140 dB SPL at 2 m [34]. For a typical background noise level of 50 dB SPL, the SNR is 90 dB. In comparison, the MLS method with order 16 and no repetition has only 60.5 dB SNR after parameter optimization and compensation for nonlinearities [11]. Therefore, inadequate signal energy is not an issue for a starter pistol. Third, a starter pistol blast approximates a point source more closely than any other excitation method considered. This is good for comparing the measured impulse response with the simulation from the image source method because the latter assumes a point source.

Figure 1 compares the frequency response of a starter pistol, estimated as the average of ten pistol shots in an anechoic chamber, to the frequency response of the ambient noise in a room response test chamber (a 2 m plywood cube). The ambient noise is 70 dB SPL with linear weighting, as measured with a Type 2260 B&K Modular Precision Sound Analyzer.

ISO 3382 specifies a peak SPL at least 45 dB above the background noise in the frequency range of interest [7]. Even for a noisy 70 dB SPL environment, the SNR of a starter pistol shot exceeds 45 dB for the frequency range 280 Hz to 11 kHz, and 30 dB for 110 Hz to 20.5 kHz (Fig. 1).

According to the excitation signal requirements described in Sec. 2.1, the starter pistol still lacks repeatability and omnidirectionality. To use it for room response measurement, experimental methods must be developed to control these two deficiencies.

#### 3.1.2. *Transfer function measurement methods*

Our experiment measures the room impulse response of a 2 m plywood-walled cube. The cube contains only a microphone and starter pistol; all other measuring equipment is located outside to avoid any disturbance caused by obstacles inside the cube. The starter pistol is mounted on the end of a sturdy pipe and triggered from outside the cube by pulling a cable.

There are two different starter pistol and microphone positions, resulting in a  $2 \times 2$  matrix transfer

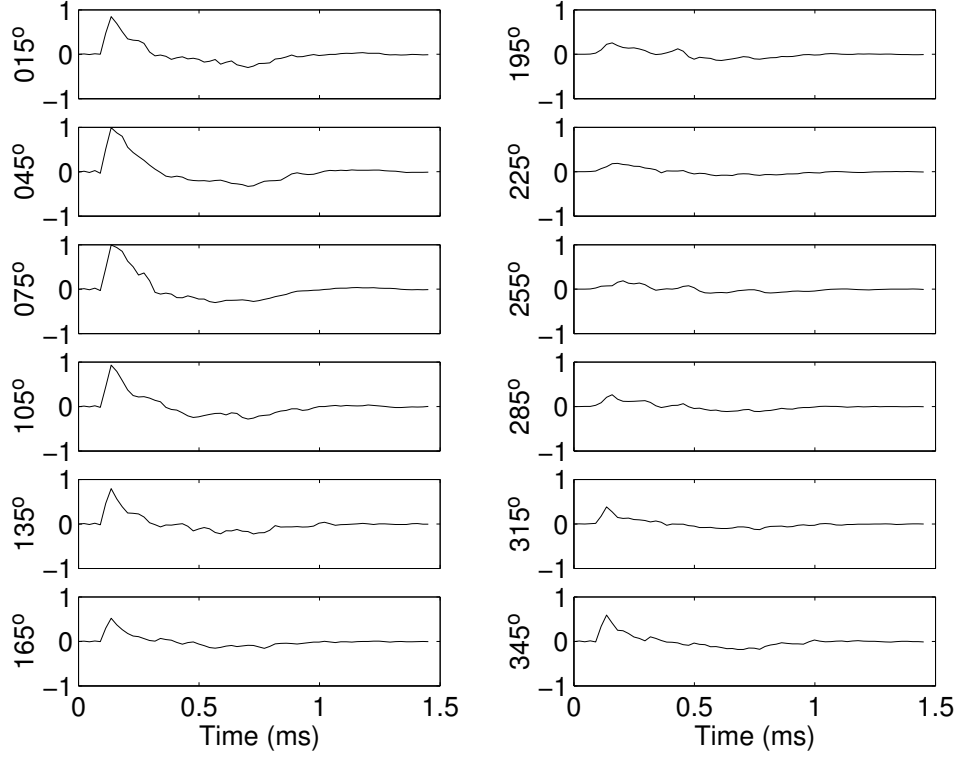


Fig. 6: Gun-Related Transfer Functions (GRTFs).

function. The exact dimensions of the plywood cube are  $(L_x, L_y, L_z) = (1.84 \text{ m}, 1.79 \text{ m}, 1.83 \text{ m})$ ; table 1 lists the positions of the starter pistol and microphone. Note that the center of the cube is  $(0 \text{ m}, 0 \text{ m}, 0 \text{ m})$ .

Since waveforms of individual pistol shots are not identical (Fig. 2), we average multiple measurements at the same location. This repetition has two benefits. First, we can assume that the averaged impulse response is due to the averaged excitation. This reduces measurement irregularity, improving repeatability. Second, SNR improves because the background noise can be assumed to be independent of room impulse response.

Like any excitation signal, a starter pistol blast is directional. This variation of signal with respect to angle we label Gun-Related Transfer Function (GRTF). Figure 6 shows the first 1.5 ms of each GRTF.

Figure 7 shows the directional pattern computed from the energy at each angle.

To measure the response of the room to an omnidirectional source, the position of the starter pistol is fixed and the barrel is rotated to positions  $30^\circ$  apart, where  $0^\circ$  is directly toward the microphone, averaging five impulse responses at each angle. The experiment uses 12 rotation angles, so a total of 60 shots determine the room impulse response from one point to another point.

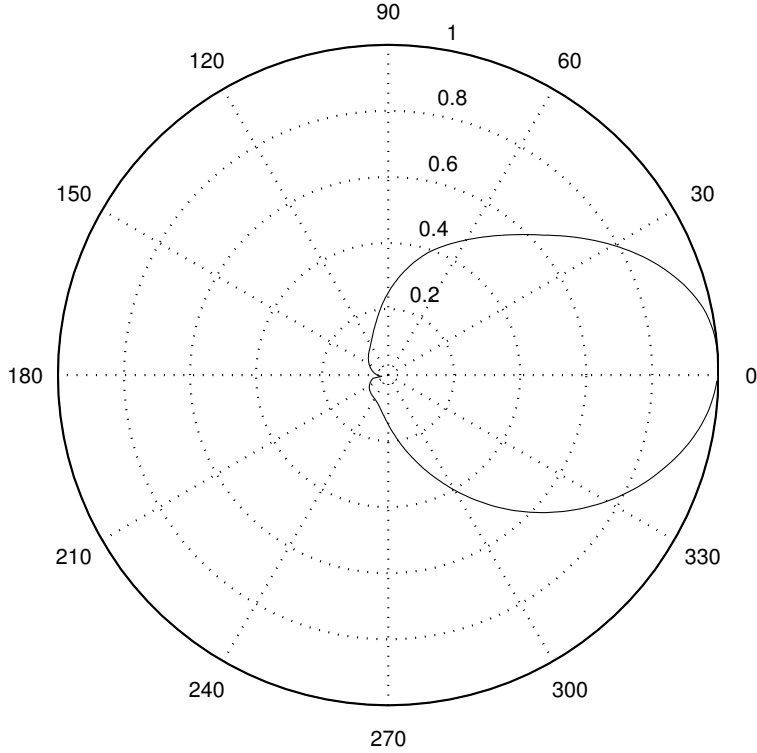


Fig. 7: Directional pattern of the starter pistol blast in normalized linear scale.

### 3.2. Room response simulation

It is impractical to directly measure all the room impulse responses from every loudspeaker position to every mesh point: only eight loudspeakers and a  $10 \times 10 \times 10$  mesh demand 8000 experiments. Instead, inverse transfer functions are derived from approximate room responses simulated with the image source method. This then demands verification of the simulation, using error metrics to compare corresponding pairs of measured and simulated responses.

Parameters of the image source simulation include the room dimensions, the position of the sound source and receivers, the speed of sound (dependent on temperature and relative humidity[35]), and the reflection coefficient  $r$  of the wall material (Eq. (1)). Although  $r$  varies with frequency, modeling the frequency dependence greatly increases the computational cost of the simulation. All simulations reported in this paper therefore assume a frequency-independent  $r$ , related to the average Sabine absorptivity  $\bar{a}$ : [4]

$$\bar{a} = 1 - r^2$$

The value of  $\bar{a}$  is optimized experimentally.

The simulation uses a sampling frequency of 44.1 kHz. The length of the simulated impulse response is 65536 samples, about 1.5 seconds. The speed of sound is taken to be 346.58 m/s, based

on Cramer's equation evaluated at the temperature and relative humidity measured in the plywood cube (24.4°C, 37.5%) [35].

Room response simulations were evaluated using three metrics: local mean-squared error (described here), global and local dereverberation ratios (described in the next section), and remainder reverberation time (described in the next section). Mean-squared error measures time-domain similarity, i.e., how alike the amplitude-versus-time graphs of the two responses look. For an  $M$  sample interval starting at the  $k^{th}$  sample, this error is expressed as

$$E_{ms}[k] = \frac{1}{M} \sum_{n=k}^{k+M-1} \left( \frac{\hat{g}[n]}{\hat{g}_{rms}} - \frac{g[n]}{g_{rms}} \right)^2 \quad (5)$$

where  $\hat{g}[n]$  and  $g[n]$  are the simulation and measurement of the room impulse responses, and  $\hat{g}_{rms}$  and  $g_{rms}$  are their RMS values in the interval  $[k, k + M - 1]$ .

For an actual room response  $G_{orig}(z)$  and an excitation signal spectrum  $S(z)$ , the measured room response is  $G(z) = S(z)G_{orig}(z)$ . When the excitation signal is a starter pistol,  $S(z)$  may be measured by recording the pistol impulse response  $s(t)$  in an anechoic chamber; when the excitation signal is pseudo-noise or a sine sweep,  $S(z)$  must be computed by multiplying the theoretical pseudo-noise spectrum with the loudspeaker frequency response. Pseudo-noise room response measurement techniques may then compare  $G(z)S(z)^{-1}$ , the source-corrected room response, with  $\hat{G}(z)$ , the simulated room response. When  $S(z)$  is the spectrum of a starter pistol, however,  $S(z)^{-1}$  has undesirable properties (it is high-pass, noncausal, and nearly singular), so the "source-corrected" room response  $g(t) * s(t)^{-1}$  is difficult to evaluate visually. Conversely, because  $s(t)$  is impulse-like, visual comparison of the measured response  $g(t)$  with  $\hat{g}(t) * s(t)$  (the measured excitation filtered by simulated response) is natural and meaningful.

Figure 9 compares the first 20 ms of two impulse responses from starter pistol position 2 to microphone position 1 (see Fig. 8 and table 1). The upper plot shows  $g(t)$ , the average of the 60 measured impulse responses. The lower plot is  $\hat{g}(t) * s(t)$ , where  $\hat{g}(t)$  is computed using the image source method. The very close match between these two impulse responses validates both the image source method and the angle-averaged pistol measurement.

The simulation preserves the peak locations closely even after 100 ms (Fig. 10), but the visual similarity of the signals is not as great as during the first 20 ms (Fig. 9).

The increasing dissimilarity between  $g(t)$  and  $\hat{g}(t) * s(t)$  as  $t$  increases is quantified by a gradual increase in the local mean-squared error of the simulation, computed using Eq. (5) with intervals of 20 and 100 ms (Fig. 11). This time-dependent dissimilarity may be explained by considering the accumulated effect on  $g(t)$  of frequency-dependent wall reflections and air propagation filtering.  $\hat{g}(t)$  is computed using the time-domain image source method, which does not model frequency-dependent wall reflections and air propagation.

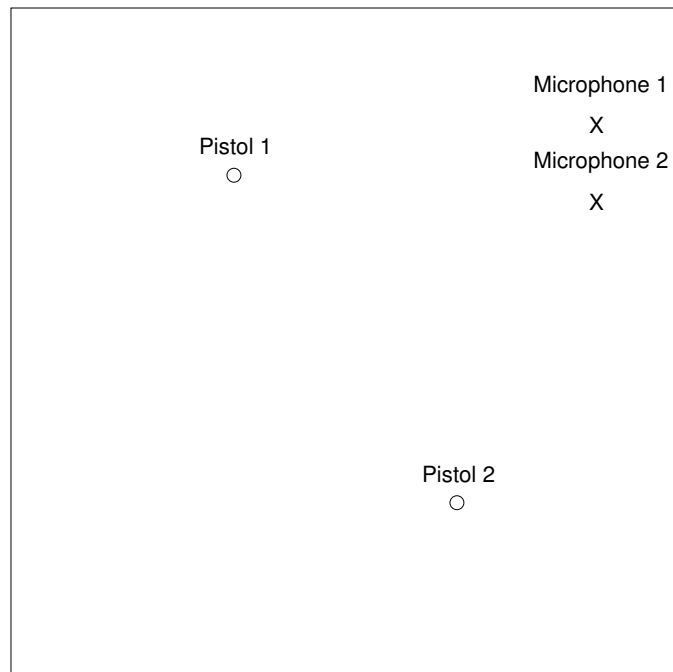


Fig. 8: Experiment setup.

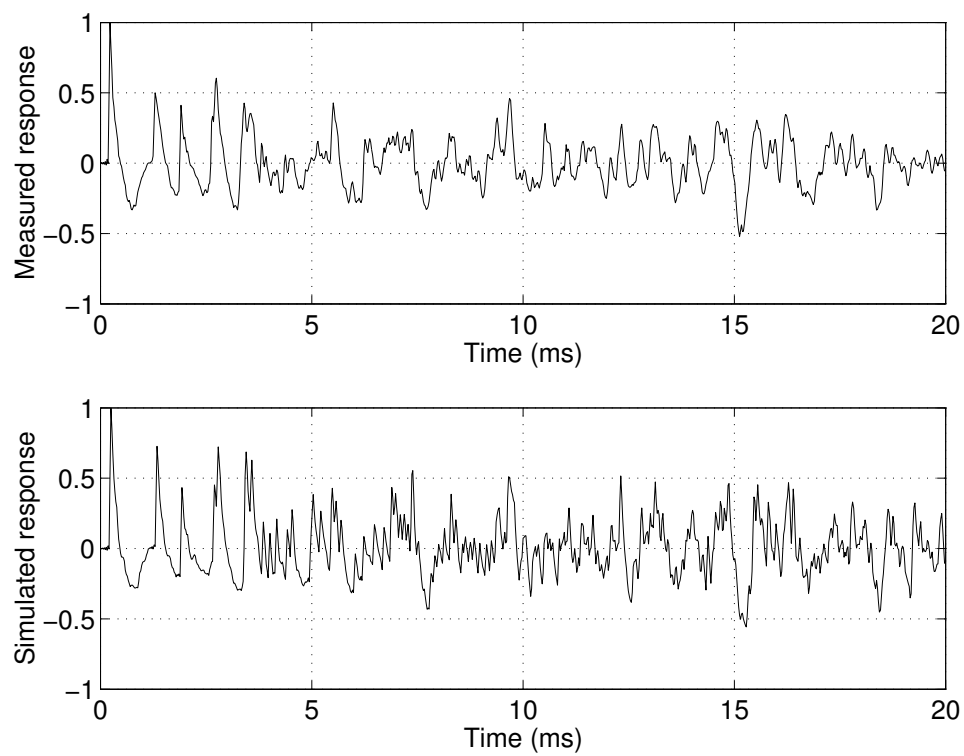


Fig. 9: First 20 ms of measured and simulated impulse responses.

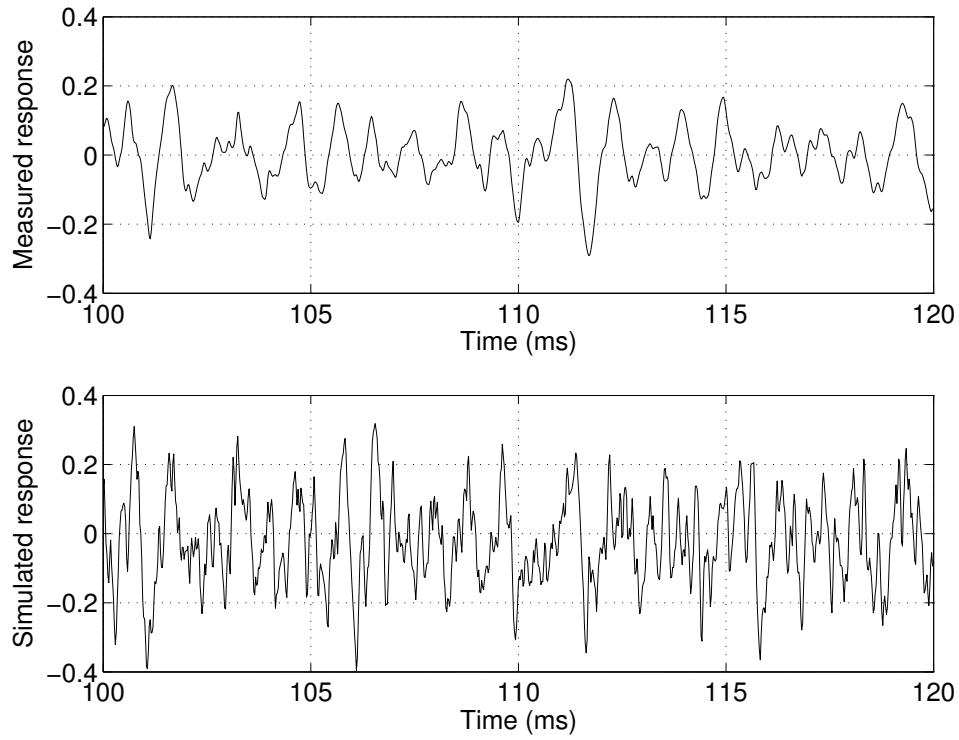


Fig. 10: Measured and simulated impulse responses after 100 ms.

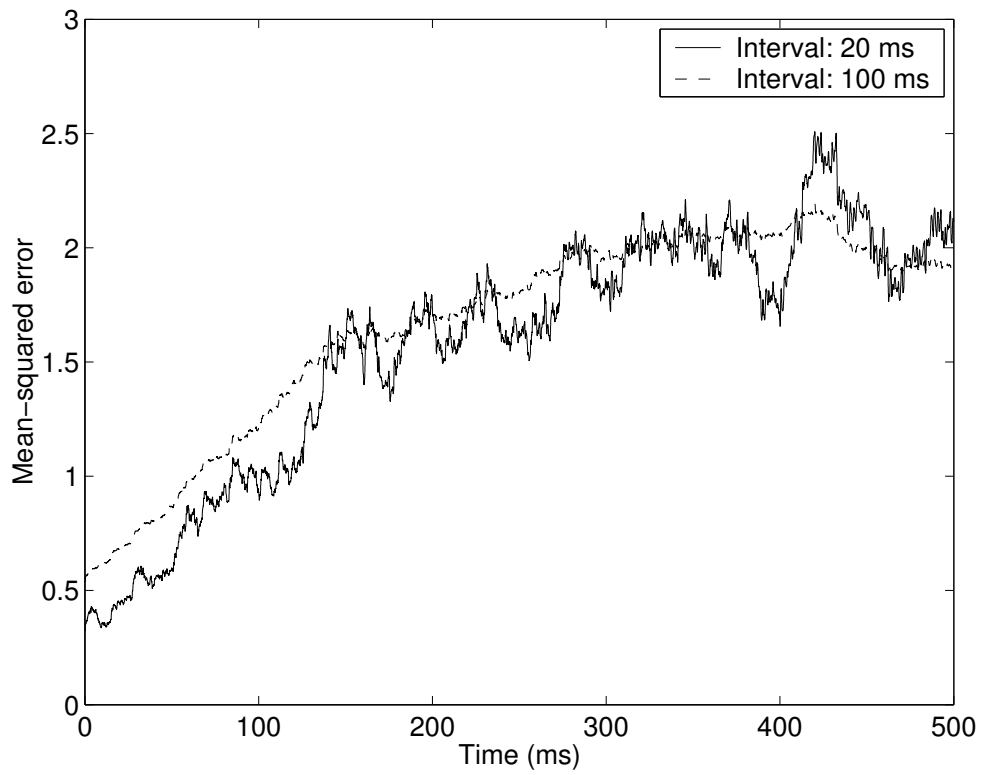


Fig. 11: Mean-squared error between simulation and measurement.



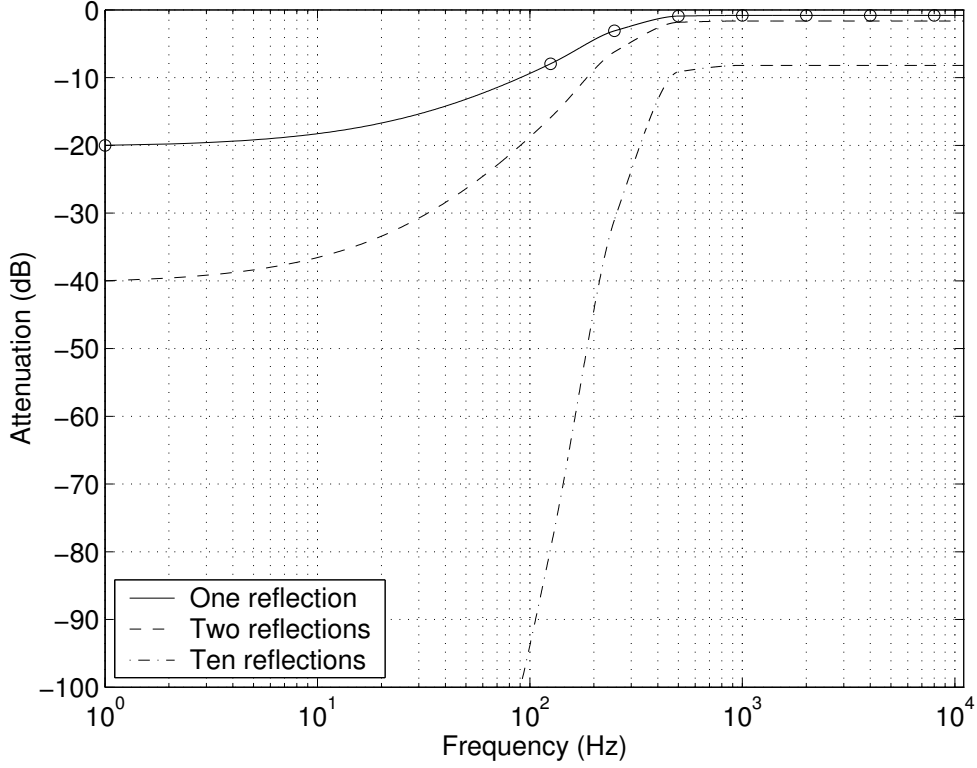


Fig. 12: Frequency response after one, two, and ten wall reflections. (Circled data points are adapted from [36].)

Figure 12 shows the filtering effect of wall reflections on the spectrum of a single acoustic ray. After only one reflection, frequencies below 10 Hz are attenuated 20 dB relative to frequencies above 100 Hz [36]. After ten reflections (70 to 100 ms), frequencies below 100 Hz are effectively zeroed. Figure 13 shows the filtering effect of propagation through air at 20° C and 30% relative humidity [37]. After 34.3 m (100 ms), spectral components at 10 kHz are attenuated about 8 dB. The attenuation due to wall reflections and air propagation is enormous even after 100 ms.

### 3.3. Room response inversion

Room responses simulated using the image source method are next inverted using the method of regularized inversion with modeling delay [3]. Experiments indicate that effective inversion requires  $\beta > 0$ , but that the exact value of  $\beta$  in the range  $10^{-4} \leq \beta \leq 1$  has little effect on inversion performance. The value of the modeling delay  $D$  is more important. Inversion results improve almost monotonically as  $D$  increases, suggesting that  $D$  be the longest modeling delay imperceptible to users. Results in this paper use  $\beta = 10^{-2}$  and  $D = 500$  ms. Finally, Eq. (4) may be used for either scalar inversion (one speaker, one control point) or matrix room response inversion ( $L$  speakers,  $M$  control points). This paper reports results of both scalar and matrix inversion experiments, where matrix inversion is performed with

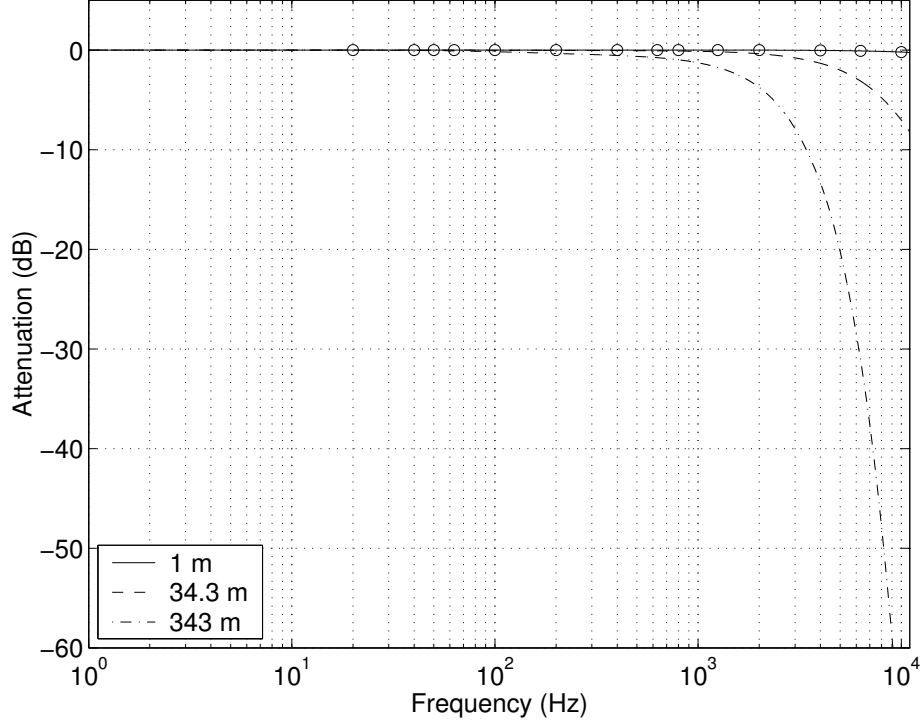


Fig. 13: Frequency response of propagation through air at 20 deg C, 30% relative humidity after 1 m, 34.3 m, and 343 m. (Circled data points are adapted from [37].)

$L = 2$ ,  $M = 2$  using the geometry shown in Fig. 8 and table 1.

### 3.3.1. Evaluation of room impulse response inversion

Room response inversion can eliminate the perceptual “signature” of a room by attenuating early echoes; it can also reduce long-term reverberant energy.

The early echoes should be well suppressed because they characterize the perceived geometry of the room. The later portion of the room response is related more to wall material and room size than to specific room geometry.

Assuming that the desired signal  $x(t)$  at a certain location is an impulse, the output  $\hat{x}(t)$  at that location needs to be as close to an impulse as possible: it should contain as little energy as possible at time  $t \neq 0$ . The output is expressed as  $\hat{X} = G\hat{H}X$  where  $G$  is a measured impulse response and  $\hat{H}$  is the approximate inverse filter created from the simulation  $\hat{G}$  using Eqs. (2), (3), and (4). The time-domain expression of the output is

$$\hat{x}(t) = g(t) * \hat{h}(t) * x(t)$$

or, for matrix inversion experiments,

$$\hat{x}_k(t) = \sum_{j=1}^L \sum_{i=1}^M g_{kj}(t) * \hat{h}_{ji}(t) * x_i(t)$$

To claim that the inverse filter dereverberates the room impulse response, for an input  $x(t) = \delta(t)$ , the filtered output  $\hat{x}(t) = \hat{h}(t) * g(t)$  should be similar to a delayed impulse,  $\hat{x}(t) \approx \delta(t - D)$ . The success of dereverberation may be measured by computing the residual energy in the signal  $\hat{x}(t)$  at times  $|t - D| > T_{min}$ , for some small value of  $T_{min}$ . The residual energy in  $\hat{x}(t)$  is computed as

$$E_{resid}(\infty) = \int_{T_{min} < |t-D|} \hat{x}^2(t) dt$$

“Early echoes” may be defined to be causal or noncausal echoes within a time window  $|t - D| < T$ . The residual energy within  $T$  seconds is computed as

$$E_{resid}(T) = \int_{T_{min} < |t-D| < T} \hat{x}^2(t) dt$$

The efficacy of the dereverberation is described by the “dereverberation ratio” (DR): the ratio of the original room response energy  $\int_{T_{min}}^T g^2(t) dt$  to the residual energy, thus,

$$DR(\infty) = 10 \log_{10} \frac{\int_{T_{min}}^{\infty} g^2(t) dt}{\int_{T_{min} < |t-D|} \hat{x}^2(t) dt}$$

$$DR(T) = 10 \log_{10} \frac{\int_{T_{min}}^T g^2(t) dt}{\int_{T_{min} < |t-D| < T} \hat{x}^2(t) dt}$$

For the output  $\hat{x}(t)$  to have less energy than the measured impulse response  $g(t)$ , both decibel ratios should be positive. They can therefore be used to evaluate and optimize the simulation and inversion of the room impulse responses.

Simulation and inversion can also be evaluated using the remainder reverberation time  $T_L$ , defined implicitly as

$$L = 10 \log_{10} \frac{\int_0^{\infty} g^2(t) dt}{\int_{T_L}^{\infty} \hat{x}^2(t) dt}$$

The remainder reverberation times  $T_{10}$ ,  $T_{20}$ , and  $T_{60}$  of both measured and dereverberated outputs will be compared. The reference for the remainder reverberation time is the integrated energy of the measured room impulse response  $g(t)$ .

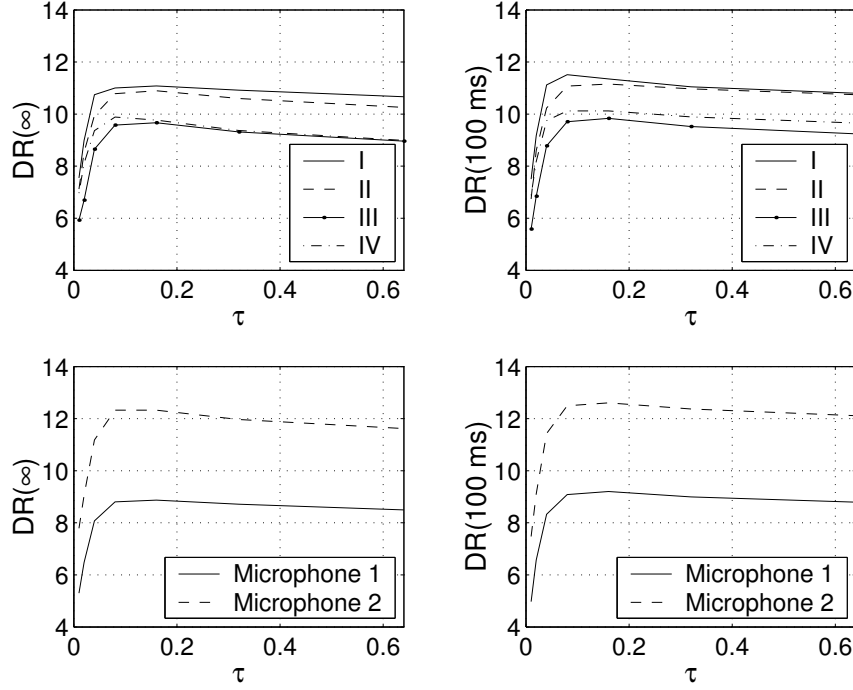


Fig. 14: Dereverberation ratios with respect to the time constant. Upper graphs, scalar inversion; lower graphs, matrix inversion.

### 3.3.2. Optimization of the window for for impulse response inversion

An inverse filter created using a complete 1.5 second simulation of the room response fails: the energy of the dereverberated output exceeds the energy of the measured impulse response.

The mean-squared error with respect to time ( $E_{ms}$ ) indicates that the accuracy of the image source simulation decreases with time (Fig. 11). This suggests that the dereverberation ratio may improve by applying a tapering window, such as an exponential with time constant  $\tau$ :

$$\tilde{g}(t) = e^{-t/\tau} \hat{g}(t)$$

Figure 14 shows the dereverberation ratios  $DR(\infty)$  and  $DR(100 \text{ ms})$  for both scalar and matrix inversion, using  $\tilde{g}(t)$  instead of  $\hat{g}(t)$  in order to create the inverse filter, with values of  $\tau = 0.01, 0.02, 0.04, 0.08, 0.16, 0.32$ , and  $0.64 \text{ s}$ .

According to the dereverberation ratios depicted above,  $\tau = 0.06 \text{ s}$  is close to optimal.

## 4. Results

Two measures are used to discuss the inversion results. First, the total and the early dereverberation ratios  $DR(\infty)$  and  $DR(T)$  are compared. Second, the remainder reverberation times  $T_{10}$ ,  $T_{20}$ , and  $T_{60}$

Table 1: Positions (in meters) of pistol and microphone in plywood cube.

	Position 1	Position 2
Pistol	(0.26, 0.30, -0.15)	(-0.26, -0.30, -0.15)
Microphone	(-0.57, 0.58, 0.31)	(-0.39, 0.58, 0.31)

of measured and dereverberated responses are compared.

Results of scalar inversion for four different impulse responses and of matrix inversion of a  $2 \times 2$  matrix transfer function are presented here. The four different room response geometries used for both scalar and matrix inversion may be numbered as follows, with reference to Fig. 8 and table 1: Impulse response number I, pistol 1 to microphone 1; II, pistol 1 to microphone 2; III, pistol 2 to microphone 1; and IV, pistol 2 to microphone 2. For  $2 \times 2$  matrix inversion, room responses at microphone location 1 and 2 are called microphone 1 and microphone 2 respectively.

Section 4.1 describes experiments designed to optimize and validate the image source method. Section 4.2 describes scalar inversion results with and without windowing the simulated room response. Section 4.3 describes  $2 \times 2$  matrix inversion results with windowing.

#### 4.1. Optimization of absorption coefficient

When all interior surfaces of the room are covered with the same material and the reverberation time is known, average Sabine absorptivity  $\bar{a}$  is given directly by Sabine’s formula

$$\bar{a} = \frac{0.161V}{ST_{60}}$$

where  $V$  and  $S$  are the volume and the surface area of the room respectively [36].

The measured  $T_{60}$  of the 2 m plywood cube using Schroeder’s integration formula [38] is 1.32 s, yielding  $\bar{a} = 0.0407$ . Since this is merely an estimation from Sabine’s formula, it was bracketed with values 0.01, 0.02, 0.04, 0.08, and 0.16.

Figure 15 shows that dereverberation ratios are not affected by the modeled absorption coefficient  $\bar{a}$ . This indicates that the phase information of the room impulse response is more important than the magnitude information, i.e., for inversion the exact timing of the reflections is more important than their magnitudes.

#### 4.2. Scalar inversion with and without windowing

Scalar inversion was performed both without and with exponential windowing of the simulated response. Figure 16 depicts the measured impulse response and the response “dereverberated” without windowing

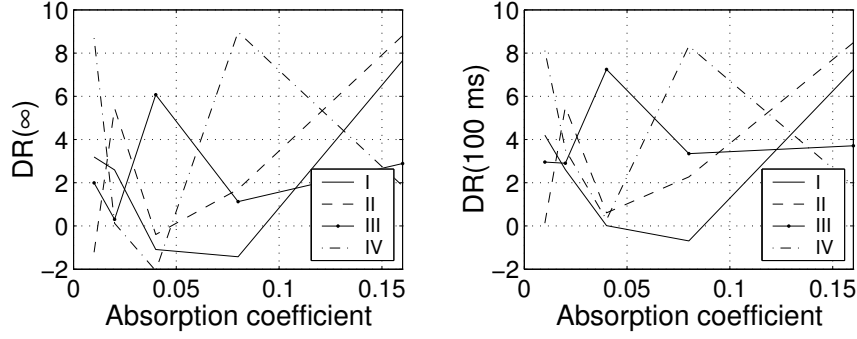


Fig. 15: Dereverberation ratios with respect to absorption coefficient  $\bar{a}$ .

Table 2: Dereverberation ratios in dB of dereverberated impulse responses.

	Non-windowed		Windowed	
	$DR(\infty)$	$DR(100 \text{ ms})$	$DR(\infty)$	$DR(100 \text{ ms})$
I	-8.95	-9.03	10.98	11.45
II	-10.54	-9.85	10.56	10.84
III	-10.11	-10.04	8.11	8.30
IV	-8.88	-8.60	10.56	10.84

from starter pistol location 1 to microphone location 2 (impulse response number II). Table 2 shows that the supposedly dereverberated impulse responses have approximately 10 dB more energy than the measured impulse responses; so dereverberation fails when no tapering window is applied to the simulated impulse responses.

Figure 17 depicts the results of dereverberation, where simulated impulse responses are windowed by an exponential window with time constant  $\tau = 0.06$  s. Table 2 shows that the dereverberated impulse responses have from 8.11 to 10.98 dB less energy than the measured impulse responses; dereverberation works.

Figure 18 shows integrated energy decay curves of four different dereverberated impulse responses with respect to the measured impulse responses; table 3 lists the dereverberation times of scalar inversion according to these decay curves.

#### 4.3. Matrix inversion with windowed simulation

Figures 19 and 20 depict  $2 \times 2$  matrix inversion results; dereverberation ratios are in table 4. Remainder reverberation energy decay curve and corresponding remainder reverberation times ( $T_{10}$ ,  $T_{20}$ , and  $T_{60}$ ) are shown in Fig. 21 and table 5.

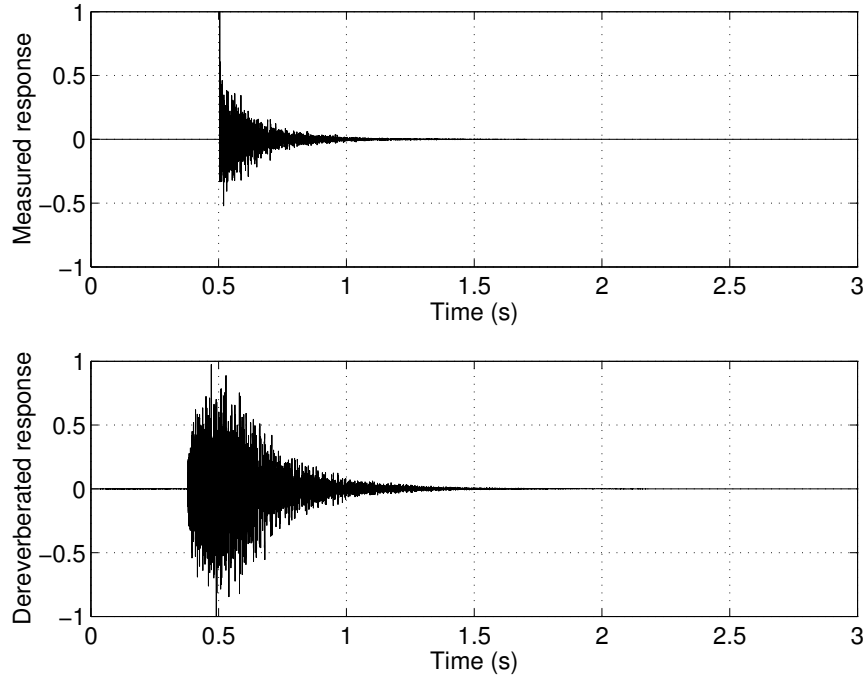


Fig. 16: Linear plots of measured and dereverberated impulse responses (scalar inversion; impulse response number III). No windowing is applied to the simulated impulse response  $\hat{g}(t)$ .

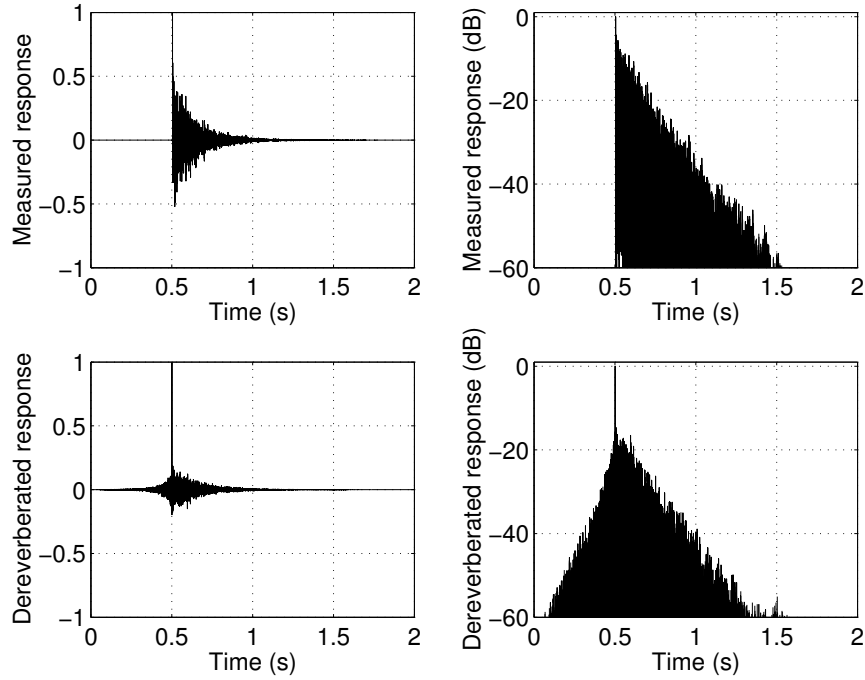


Fig. 17: Measured and dereverberated impulse responses (scalar inversion; impulse response number III). An exponential window with time constant  $\tau = 0.06$  s is applied to the simulated impulse response  $\hat{g}(t)$ .

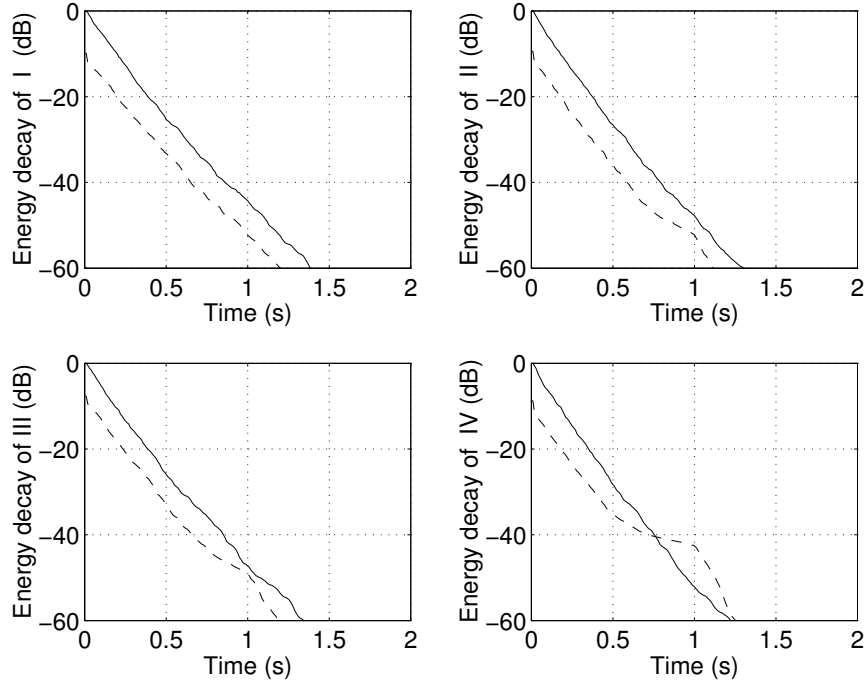


Fig. 18: Integrated energy decay curves for scalar inversion. Solid line is measured response; dashed line is dereverberated response.

Table 3: Remainder reverberation times  $T_{10}$ ,  $T_{20}$ , and  $T_{60}$ , in seconds, of measured and dereverberated impulse responses; scalar inversion.

	Measured responses			Dereverberated responses		
	$T_{10}$	$T_{20}$	$T_{60}$	$T_{10}$	$T_{20}$	$T_{60}$
I	0.20	0.39	1.39	0.02	0.20	1.21
II	0.18	0.38	1.31	0.02	0.18	1.12
III	0.19	0.39	1.35	0.04	0.24	1.19
IV	0.18	0.36	1.23	0.02	0.19	1.26

Table 4: Dereverberation ratios in dB of dereverberated impulse responses; matrix inversion.

	Microphone 1	Microphone 2
$DR(\infty)$	8.64	12.04
$DR(100 \text{ ms})$	8.83	12.19



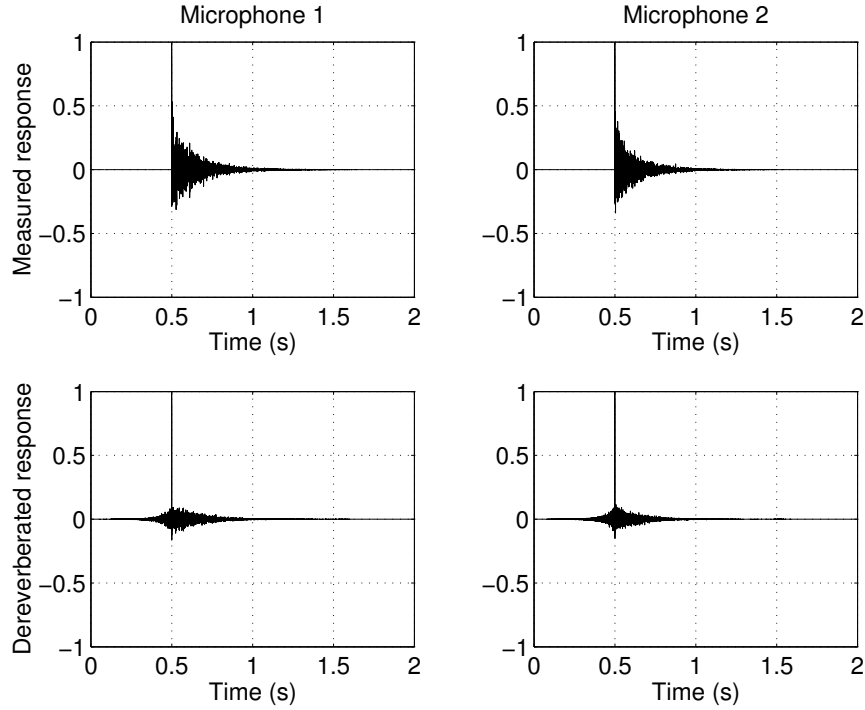


Fig. 19: Linear plots of measured and dereverberated impulse responses ( $2 \times 2$  matrix inversion). An exponential window with time constant  $\tau = 0.06$  s is applied to the simulated impulse response  $\hat{g}(t)$ .

Table 5: Remainder reverberation times  $T_{10}$ ,  $T_{20}$ , and  $T_{60}$ , in seconds, of measured and dereverberated impulse responses; matrix inversion.

	Measured responses		Dereverberated responses	
	Microphone 1	Microphone 2	Microphone 1	Microphone 2
$T_{10}$	0.19	0.16	0.02	0.02
$T_{20}$	0.39	0.36	0.26	0.20
$T_{60}$	1.37	1.22	1.26	1.27

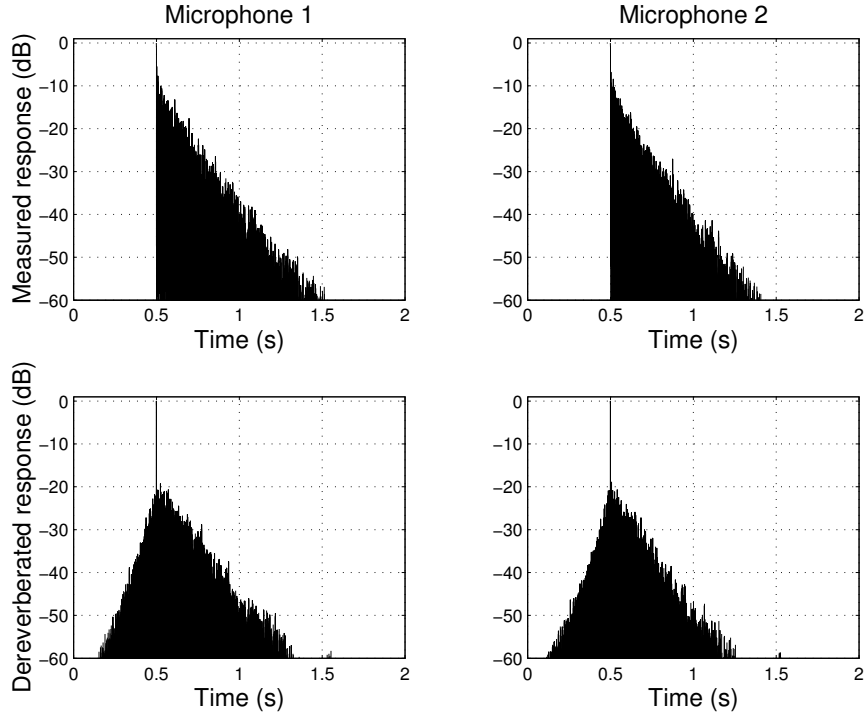


Fig. 20: Decibel plots of measured and dereverberated impulse responses ( $2 \times 2$  matrix inversion). An exponential window with time constant  $\tau = 0.06$  s is applied to the simulated impulse response  $\hat{g}(t)$ .

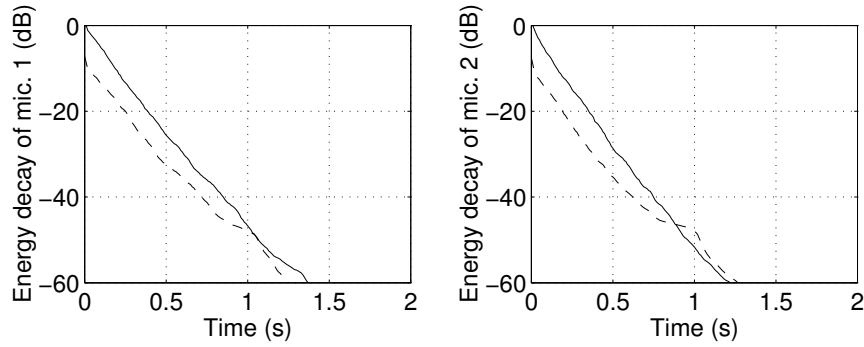


Fig. 21: Integrated energy decay curves for  $2 \times 2$  matrix inversion. Solid line is measured response; dashed line is dereverberated response.

## 5. Conclusion

This paper describes experiments in open-loop room response inversion for the purpose of headphone-free virtual reality audio display. Room responses were simulated using the image source method and inverted using a regularized Fourier transform inversion with a modeling delay of 500 ms. Scalar room response inversion provided an average of 10.1 dB of short-term dereverberation (early echoes within 100 ms of the direct sound), and 10.4 dB of long-term dereverberation. Matrix room response inversion (two inputs, two outputs) provided an average of 10.5 dB short-term and 10.3 dB long-term dereverberation.

## 6. Acknowledgments

This work was supported in part by a grant from the University of Illinois Research Board, and in part by funding from the University of Illinois Beckman Institute. We thank Hank Kaczmarski for hardware assistance.

## 7. References

- [1] C. Cruz-Neira, D. J. Sandin, and T. A. DeFanti, “Surround-screen projection-based virtual reality: the design and implementation of the CAVE,” *Proc. ACM Special Interest Group on Computer Graphics and Interactive Techniques (SIGGRAPH)*, 135–142 (1993).
- [2] M. Miyoshi and Y. Kaneda, “Inverse filtering of room acoustics,” *IEEE Trans. Acoustics, Speech and Signal Proc.* **36**(2), 145–152 (1988).
- [3] O. Kirkeby, P. A. Nelson, H. Hamada, and F. Orduna-Bustamente, “Fast deconvolution of multichannel systems using regularization,” *IEEE Trans. Speech and Audio Processing* **6**(2), 189–194 (1998).
- [4] J. B. Allen and D. A. Berkley, “Image method for efficiently simulating small-room acoustics,” *J. Acoust. Soc. Am.* **65**(4), 912–915 (1979).
- [5] S. T. Neely and J. B. Allen, “Invertibility of a room impulse response,” *J. Acoust. Soc. Am.* **66**(1), 165–169 (1979).
- [6] A. Omoto, C. Hiratsuka, H. Fujita, T. Fukushima, M. Nakahara, and K. Fujiwara, “Similarity

evaluation of room acoustic impulse responses: Visual and auditory impressions,” J. Audio. Eng. Soc. **50**(6), 451–457 (2002).

- [7] ISO 3382, *Acoustics - Measurement of the reverberation time of rooms with reference to other acoustical parameters*, ISO, 1997.
- [8] M. R. Schroeder, “Integrated-impulse method measuring sound decay without using impulses,” J. Acoust. Soc. Am. **66**(2), 497–500 (1979).
- [9] D. D. Rife and J. Vanderkooy, “Transfer-function measurement with maximum-length sequences,” J. Audio. Eng. Soc. **37**(6), 419–444 (1989).
- [10] J. Vanderkooy, “Aspects of MLS measuring systems,” J. Audio. Eng. Soc. **42**(4), 219–231 (1994).
- [11] G.-B. Stan, J.-J. Embrechts, and D. Archambeau, “Comparison of different impulse response measurement techniques,” J. Audio. Eng. Soc. **50**(4), 249–262 (2002).
- [12] C. Dunn and M. O. Hawksford, “Distortion immunity of MLS-derived impulse response measurements,” J. Audio. Eng. Soc. **41**(5), 314–335 (1993).
- [13] N. Ream, “Nonlinear identification using inverse-repeat m sequences,” Proc. IEE (London) **117**(1), 213–218 (1970).
- [14] P. A. N. Briggs and K. R. Godfrey, “Pseudorandom signals for the dynamic analysis of multivariable systems,” Proc. IEE **113**, 1259–1267 (1966).
- [15] H. R. Simpson, “Statistical properties of a class of pseudorandom sequence,” Proc. IEE (London) **113**, 2075–2080 (1966).
- [16] C. Bleakley and R. Scaife, “New formulas for predicting the accuracy of acoustical measurements made in noisy environments using the averaged m-sequence correlation technique,” J. Acoust. Soc. Am. **97**(2), 1329–1332 (1995).
- [17] H. Alrutz and M. R. Schroeder, “A fast Hadamard transform method for the evaluation of measurements using pseudorandom test signals,” Proc. 11th Int. Congress on Acoustics (Paris) **6**, 235–238 (1983).

- [18] M. Cohn and A. Lempel, "On fast M-sequence transforms," IEEE Trans. Inform. Theory **23**(1), 135–137 (1977).
- [19] W. D. T. Davies, "Generation and properties of maximum-length sequences, part 1," Control **10**(96), 302–304 (1966).
- [20] W. D. T. Davies, "Generation and properties of maximum-length sequences, part 2," Control **10**(97), 364–365 (1966).
- [21] W. D. T. Davies, "Generation and properties of maximum-length sequences, part 3," Control **10**(98), 431–433 (1966).
- [22] D. D. Rife, "Modulation transfer function measurement with maximum-length sequences," J. Audio. Eng. Soc. **40**(10), 779–790 (1992).
- [23] M. Vorländer and M. Kob, "Practical aspects of MLS measurements in building acoustics," Appl. Acoustics **52**(3-4), 239–258 (1997).
- [24] R. Burkard, Y. Shi, and K. E. Hecox, "A comparison of maximum length and Legendre sequences for the derivation of brain-stem auditory-evoked responses at rapid rates of stimulation," J. Acoust. Soc. Am. **87**(4), 1656–1664 (1990).
- [25] N. Aoshima, "Computer-generated pulse signal applied for sound measurement," J. Acoust. Soc. Am. **69**(5), 1484–1488 (1981).
- [26] A. J. Berkhout, D. de Vries, and M. M. Boone, "A new method to acquire impulse responses in concert halls," J. Acoust. Soc. Am. **68**(1), 179–183 (1980).
- [27] A. Farina, "Simultaneous measurement of impulse response and distortion with a swept-sine technique," J. Audio. Eng. Soc. **48**, 350 (2000).
- [28] R. Rabenstein and A. Zayati, "A direct method to computational acoustics," IEEE Proc. Int. Conf. Acoustics, Speech and Signal Processing (ICASSP 99) **2**, 957–960 (1999).

- [29] T. Schetelig and R. Rabenstein, “Simulation of three-dimensional sound propagation with multi-dimensional wave digital filters,” IEEE Proc. Int. Conf. Acoustics, Speech and Signal Processing (ICASSP 98) **6**, 3537–3540 (1998).
- [30] A. Krokstad, S. Strøm, and S. Sørsdal, “Calculating the acoustical room response by the use of a ray tracing technique,” J. Sound Vib. **8**(1), 118–125 (1968).
- [31] J. Borish, “Extension of the image model to arbitrary polyhedra,” J. Acoust. Soc. Am. **75**(6), 1827–1836 (1984).
- [32] H. Lee and B.-H. Lee, “An efficient algorithm for the image model technique,” Applied Acoustics **24**, 87–115 (1988).
- [33] P. A. Nelson, H. Hamada, and S. J. Elliott, “Adaptive inverse filters for stereophonic sound reproduction,” IEEE Trans. Signal Processing **40**(7), 1621–1632 (1992).
- [34] *Database for assessing the annoyance of the noise of small arms*, United States Army Environmental Hygiene Agency, 1983.
- [35] O. Cramer, “The variation of the specific heat ratio and the speed of sound in air with temperature, pressure, humidity, and CO<sub>2</sub> concentration,” J. Acoust. Soc. Am. **93**(5), 2510–2514 (1993).
- [36] L. E. Kinsler, A. R. Frey, A. B. Coppens, and J. V. Sanders, *Fundamentals of Acoustics*, 4th ed. (Wiley and Sons, Inc., New York, 2000).
- [37] *CRC Handbook of Chemistry and Physics*, 79th ed., edited by D. R. Lide (CRC Press, Boca Raton, 1998).
- [38] M. R. Schroeder, “New method of measuring reverberation time,” J. Acoust. Soc. Am. **37**(3), 409–412 (1965).